Some Properties of Deep Stratiform Ice Cloud Revealed by 95 GHz GKSS Cloud Radar - A case study

Y. Fujiyoshi,
Inst. Low Temp. Sci., Hokkaido Univ., Sapporo, JAPAN
M. Quante, O. Danne, and E. Raschke
Inst. Atmos. Phys., GKSS Res. Center, Geesthacht, Germany

Abstract

This paper presents a case study of a deep stratiform cloud observed with a 95 GHz polarimetric Doppler radar on 06 Dec., 1995, at Geesthacht, Germany. The levels of echo top and bottom were ~ 5.15 km (-30 ℃) and ~1 km (-7 ℃), respectively. The radar signal contained convective echoes above ~4.5 km, and streaks between 3 and 4.5 km. Another thin stratiform radar echo below 2.5 km was also observed. The estimated vertical air velocity indicated the existence of wave motion (wavelength ~3.6 km) of air in the streak region. The vertical air velocity showed convective-scale (0.5 ~ 1 km) fluctuations in the convective echo region. The general time-trend of vertical air velocity correlated well with the wave motion of air in the lower convective region. The intermittent updraught apparently originated at the crest of the wave. In addition, smaller-scale (<100m) but strong up- and downdraughts were observed near the cloud top, where the bulk Richardson number was ~1, mainly due to the strong wind shear. Their vertical air velocities did not correlate with the wave motion of air below.

1 Introduction

Millimeter-wave radars are quite sensitive to small hydrometeors, and provide excellent spatial resolution and minimal susceptibility. They are currently being applied to studies of microphysics, dynamics and turbulence of various kinds of clouds (e.g., Pazmany et al., 1994; Bluestein et al., 1995; Clothiaux et al., 1995; Syrett et al., 1995, Uttal et al., 1995, Danne et al., 1996). Another advantage of mm-wave radars is their mechanical compactness, which allows them to be operated from mobile ground-based, airborne, and space-based platforms, as well as from ships.

The development of solid-state mm-wave components and high-power klystron amplifiers has spurred the evolution of reliable, coherent radars operating up to 95 GHz (W-band), which is about the shortest wavelength that can be used for a meteorological radar (Lhermitte, 1987 and 1988). In addition, advances in digital signal processing technology have resulted in single-card processors that can simultaneously execute algorithms to compute reflectivity, Doppler, and polarimetric quantities in real time (Pasqualucci et al., 1983; Mead et al., 1994). Using these variables, many researchers are developing various algorithms to retrieve ice/liquid water content, size distributions, number density, fall speed and shape of particles in clouds (e.g., Sassen, 1987; Matrosov et al., 1992; Russchenberg, 1993; Mead et al., 1994; Atlas et al., 1995; Brown et al., 1995; Kropfli and Kelly, 1996; Schneider and Stephens, 1995; Sekelsky and McIntosh, 1996).

A 95 GHz polarimetric Doppler radar (MIRACLE, MIllimeter RAdar for Cloud Layer Exploration) was installed at the GKSS Research Center, Geesthacht, Germany, in late 1995, to study the complex role of clouds in the climate system. During a first field test of the system, a deep stratiform ice cloud was observed at GKSS from 1603 to 1608 GMT on 06 Dec., 1995, which is subject of this paper.

2 The GKSS 95 GHz polarimetric Doppler radar

The main characteristics of the GKSS radar (MIRACLE) are shown in Table 1 (see further details in Quante et al., 1996). The beamwidth of the antenna is 0.17°, that is, 15 m at an altitude of 5 km. Basically, this radar can measure Z_{hh}, Z_{vv}, Z_{DR} and, mean Doppler velocity and spectral width by the pulse-pair method, and Doppler velocity spectrum by the FFT method.

During the observational period, the radar was fixed vertically, transmitting only vertically polarized pulses, and measuring the Doppler velocity by the pulse-pair method. The detection limit of Z_{vv} was -25 dBZ at 5 km. The radar

Table 1: Main characteristics of GKSS 95GHz radar.

Frequency	95GHz
Peak Power	~1.7kW
Duty Cycle	1.2%
Pulse Repetition Frequency	50 Hz ~ 80 kHz
Pulse Width	0.17°
Beamwidth	1.2 m
Antenna Diameter	1.2 m
Antenna Gain	60 dB
Polarization	horizontal/vertical
Cross-polarization Isolation	> 25 dB
Output Channels	$\log(\|h\|^2)$, $\log(\|v\|^2)$, I_h, Q_h, I_v, Q_v*
Dynamic Range	> 70 dB
Bandwidth	20, 10 and 2 MHz

* $|h|^2$ and $|v|^2$ are received power in horizontal and vertical receiver channel; I and Q are in-phase and quadrature components of signal phase.

system has an internal calibration loop running all the time adjusting little variations in the output power of the tube for each profile. Also, our radar has been adjusted to the calibrated one.

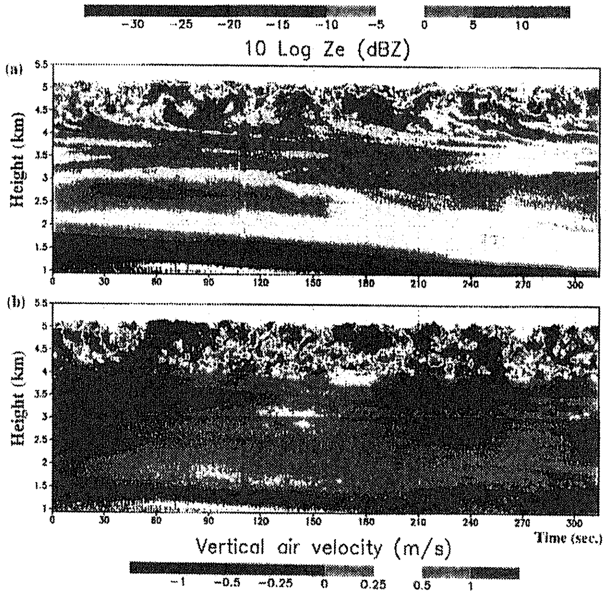

***Figure 1:** Time-height cross section of the equivalent radar reflectivity (10 Log Z_e; dBZ) (Fig. 1a) and retrieved vertical air velocity (m s^{-1}) (Fig. 1b; see section 4 for detailed explanation). Positive values in Fig. 1b indicate downward air motion. The numbers on the abscissa denote elapsed time (seconds) from the beginning of the observation (1603 GMT on 06 Dec., 1995). Height and time resolutions are 30 m and 0.3-second, respectively*

Figure 1a shows the time-height cross section of the equivalent radar reflectivity (10 Log Z_e ;dBZ). The height and time intervals were 30 m and 0.3 seconds, respectively. There were convective echoes above ~4.6 km, and streak echoes between 3 and 4.6 km. Thin streak echoes from different generating cells merged with each other (for example, see altitudes between 4.0 and 4.6 km in the first 30 seconds) and formed a long thick streak. Several streaks were detected simultaneously at different altitudes, indicating a multi-layer structure. Another thin stratiform radar echo was observed below 2.5 km.

3 Meteorological conditions

NOAA satellite imageries at 1206 GMT on 06 Dec., 1995 (not shown here), indicates that the wave-like clouds with low brightness temperature existed in the south of radar site. The METEOSAT imagery clearly shows that these clouds moved to north-north-westerly. The surface temperature at the radar site was very low (close to -10 °C), and few snow grains were temporarily observed at the ground.

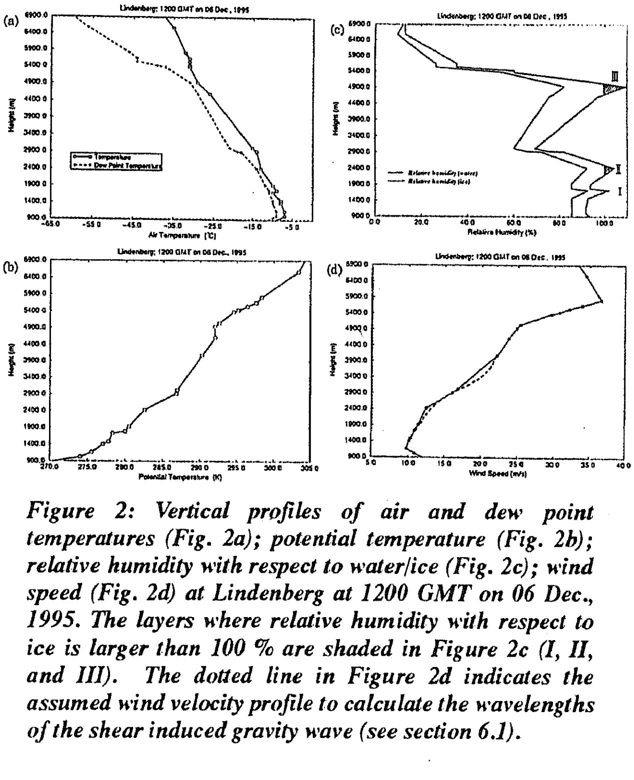

***Figure 2:** Vertical profiles of air and dew point temperatures (Fig. 2a); potential temperature (Fig. 2b); relative humidity with respect to water/ice (Fig. 2c); wind speed (Fig. 2d) at Lindenberg at 1200 GMT on 06 Dec., 1995. The layers where relative humidity with respect to ice is larger than 100 % are shaded in Figure 2c (I, II, and III). The dotted line in Figure 2d indicates the assumed wind velocity profile to calculate the wavelengths of the shear induced gravity wave (see section 6.1).*

Figure 2 shows the vertical profiles of air temperature, potential temperature, relative humidity and wind speed observed at Lindenberg upper air sounding station, about 280 km southeast of Geesthacht, at 1200 GMT on 06 Dec., 1995. A south-easterly wind blew at most levels of the troposphere with an average speed of ~20 m s^{-1}. If the air moved from Lindenberg to Geesthacht with this air speed, it would have arrived at Geesthacht at around 1600 GMT.

There were three layers (I, II and III from the bottom) in which relative humidity was saturated with respect to ice. The top of each layer was bounded by a temperature inversion or strongly stable stratification. The convective echoes occurred in layer III (~ -29 ℃). The level of echo top was ~5.15 km (-30 ℃) and apparently exceeded that of layer III. The streak echoes occurred in the dry region between layers II and III. The dry and thermally stable layer above layer III was also characterized by strong wind shear. Wind direction (not figured) changed slightly with altitude as follows: 140° in layer I, 120° in layer II, 120° in layer III, and 110° above layer III.

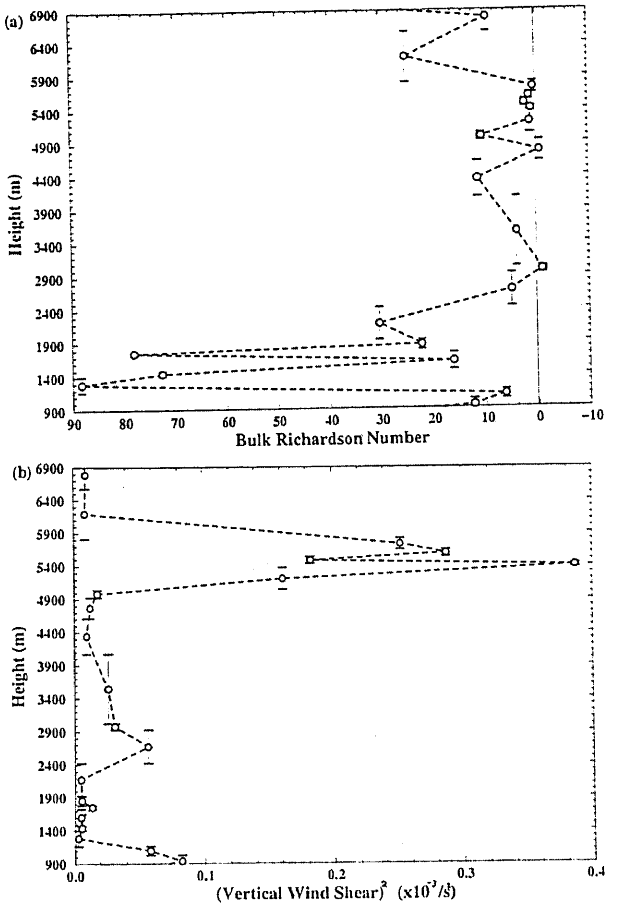

Figure 3: Vertical profiles of bulk Richardson number (Fig. 3a) and square of vertical wind shear (Fig. 3b). The vertical bar indicates the depth of the layer where each value was calculated.

Figure 3 shows the kinetic stability of the air, that is, the bulk Richardson number (Fig. 3a) and square of vertical shear of horizontal wind (s^{-2}) (Fig. 3b) calculated from the sounding data at Lindenberg. The vertical wind shear increased drastically above 5.0 km (above layer III), and the bulk Richardson number was about 1 at altitudes between 5.0 and 5.4 km (just above layer III and near the level of cloud top). Convective echoes were embedded in the layer where the bulk Richardson number was negative, that is, at altitudes between 4.6 and 4.9 km (in layer III). It was also negative between 2.9 and 3.0 km (just below streak echoes), although there were no convective echoes in this layer.

4 Estimation of vertical air velocity

The vertically directed Doppler radar measures the effective fall speed of precipitation particles. To deduce vertical air motion from the Doppler velocity (V_D), the terminal fall velocities of particles (V_t) have to be estimated. Many researchers use the formula $V_t = a\ Z_e{}^b$ to calculate V_t. If there is no vertical air motion, the Z_e- V_D relationship gives an estimate of the terminal fall velocities of particles. Further, if the mean vertical air motion is weak and the degree of fluctuation of updraught is nearly the same as that of downdraught, the regression line of Z_e- V_D would represent the Z_e- V_t relationship.

Good Z_e- V_D correlations are found between altitudes of 1.6 and 3.9 km. However, the Z_e- V_D relationship above 3.18 km (Type A) apparently differs from that below 2.55 km (Type B). The Z_e- V_t relationship for snowfall presented by Sauvageot (1992) matches well with Type A.

$$V_t = 0.817\, Z_e^{0.063} \quad (Type\ A) \quad (1)$$

$$V_t = Z_e^{0.062} \quad (Type\ B) \quad (2)$$

Relationships (1) and (2) agree well with those obtained by Heymsfield (1975b) and Carbone and Bohne (1975). They differ slightly from those of Auria and Campistron (1987), Carbone and Srivastava (1975), Herzegh and Hobbs (1975), and differ strongly from those of Matrosov et al. (1994). The difference among these Z_e- V_t relationships would be mainly caused by types of snow crystals. Type A was found in the lower stratiform region (~-10 ℃). Laboratory experiments and field observations indicate that column or thick plate crystals are the predominant type of snow crystals that grow in this temperature region (e.g., Kobayashi, 1961; Magono and Lee, 1966). Type B was found in the streak echo region (~-18 ℃), where plane dendritic crystals are known to be the predominant type of snow crystals. If the sizes are the same, column or thick plate crystals fall faster than plane dendritic crystals (e.g., Pruppacher and Klett, 1978), consistent with the observed result.

The time-height cross section of the estimated vertical air velocity is shown in Figure 1b. There is a discontinuity in the vertical air velocity at an altitude of 3.0 km, since different Z_e- V_t relationships were used below and above 3.0 km. Maximum up- and downdraught were ~1.5 m s^{-1}. Morphologically, like the echo free vault in a super cell storm, a radar echo of convex shape corresponds to a strong updraught region (e.g., at the time marks of 60~75 seconds and 240~255 seconds in Figs. 1a and 1b). It is to be noted that the sign of V_D was negative and particles actually moved upward in the strong updraught regions ($\geqq$ 1 m s^{-1}).

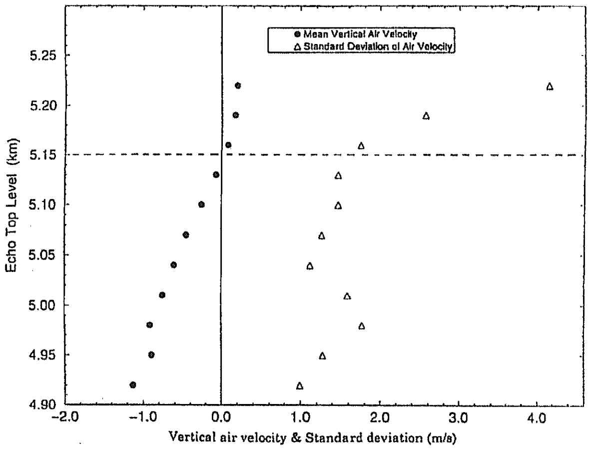

Figure 4: Relationship between echo top level and mean vertical air velocity (black circle) at each echo top level. Standard deviation of the mean air velocity is also shown (open triangles). In this figure only, positive values mean updraught and negative values mean downdraught.

Figure 1 clearly indicates a strong correlation between echo top level and vertical air motion. Figure 4, the relationship between echo top level and mean vertical air velocity at each echo top level, shows that the echo top level decreased with increasing mean downdraught velocity. When the mean vertical air velocity was 0 m s^{-1}, the level of echo top was 5.15 km, which corresponded well to the averaged echo top level. The standard deviation of the mean air velocity shown in Figure 4 increased strongly above an altitude of 5.15 km. This result suggests that turbulence caused by strong wind shear greatly affected the air velocities of overshooting air parcels.

5 Stability and turbulence

Quante et al. (1996) analyzed the cloud structure of this case by spectral analysis of radar reflectivity and Doppler velocity time series. They reported that the reflectivity as well as velocity spectrum showed higher spectral amplitudes in the convective region than in the streak region. They gave clear evidence for a -5/3th power law, indicating that microscale turbulence processes made a significant contribution to the observed velocities. Since the results of the detailed spectral analysis are reported in another paper, the turbulent structure of the cloud will be simply studied here by using pseudo turbulent kinetic energy (PTKE). The definition of PTKE follows that of normal turbulent kinetic energy and it indicates the degree of fluctuation of vertical air velocity:

$$\mathrm{PTKE} = \sum_i (w_{t=i} - \bar{w})^2/N \qquad (3)$$

Here, $\bar{w}$ and $w_{t=i}$ denote time-averaged vertical air velocity and vertical air velocity at time=i, respectively. The time step is equal to the

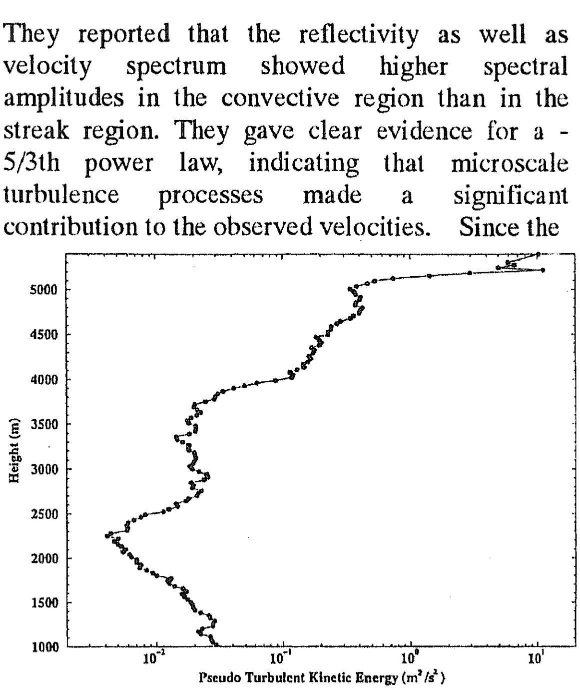

Figure 5: Vertical profiles of pseudo turbulent kinetic energy (PTKE). See text for the definition of PTKE.

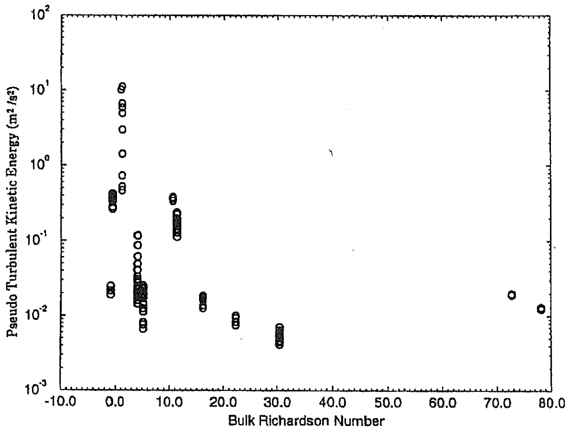

Figure 6: Dependency of PTKE on bulk Richardson number. Since the bulk Richardson number is calculated in each layer represented as vertical bar in Fig. 4, some PTKEs are plotted on the same bulk Richardson number.

sampling interval, that is, 0.3-second. Figure 5 shows the vertical profiles of time-averaged PTKE. PTKE decreased with altitude between 1.4 and 2.2 km, and increased between 2.2 and 2.8 km. It was large at altitudes above 4.0 km, and especially so above 5.0 km (near the cloud top).

The relationship between the bulk Richardson number and time-averaged PTKE is depicted in Figure 6. Although the sounding data were observed about 280 km from the radar site about 4 hours before, the figure shows that PTKE increased when the bulk Richardson number was less than 10. This result is consistent with those found in the boundary layer by many researchers (e.g., Stull, 1988).

6 Discussion

6.1 Waves and convection

In the following, we assume that the observed system did not change largely its structure during such a short period of observation time as 5 minutes.

The time-height cross section of the estimated vertical air velocity suggests the occurrence of wave motion of the air between altitudes of 2.5 and 4.0 km. Since the time interval between crests of the wave was 210 seconds and the mean air speed of the layer was 17.0 m s^{-1}, its wavelength is estimated to be ~3.6 km.

Updraughts predominated in the convective region above the region where the air moved upward in the wave. On the contrary, downdraughts predominated above the region where the air moved downward in the wave. Time changes of the vertical air velocity in Fig. 7 indicate more clearly the strong connection between the convective activity and the undulatory air motion. The amplitude of the vertical air velocity was ~ 0.1 m s^{-1} below 2.8 km and increased with altitude above 2.8 km. The short-term fluctuation of vertical air velocity between 2.8 and 3.96 km (in the wave) was smaller than that below 2.8 km. Gultepe and Starr (1995) also found that the amplitude of small-scale fluctuations was generally suppressed in larger-scale waves in cirrus clouds. Just below the convective region (H = 4.26 - 4.56 km), the general time-trend of vertical air velocity correlated well with the lower-level undulatory air motion (H = 3.66 - 3.96 km), although its fluctuation was large. In the upper half of the convective echo region (H = 4.86 - 5.16 km), however, the vertical air velocity did not correlate with the undulatory air motion, but showed strong smaller-scale (≦1 km) fluctuations.

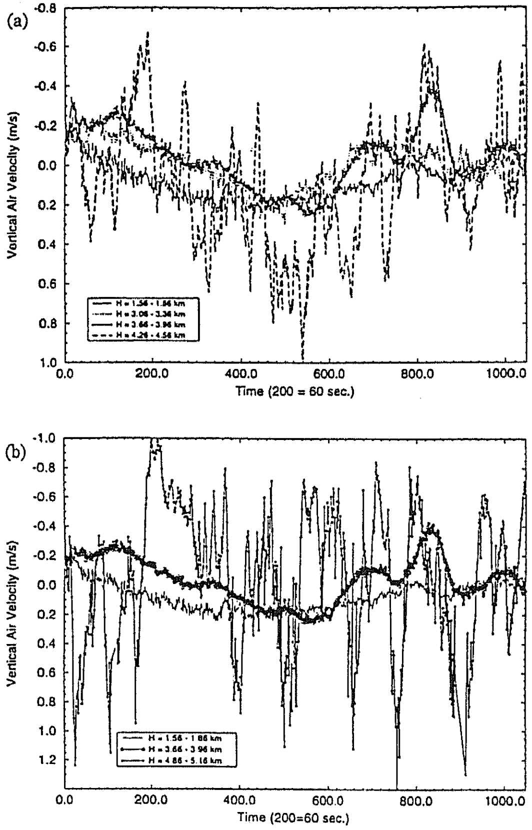

Figure 7: ***Time changes of the vertical air velocity from 1.56 to 4.56 km (a) and from 1.56 to 5.16 km (b). The vertical air velocity was averaged for layers of depth 0.3 km. The sign of the ordinate is inverted, since upward air motion is defined to be negative.***

The wave appeared in the layer with a negative bulk Richardson number and strong wind shear, that is, 7.2 x 10^{-3} s^{-1} between 2.4 and 3.0 km and 5.1 x 10^{-3} s^{-1} between 3.0 and 4.0 km. These are favorable conditions for development of a gravity wave. Following the theory of Lalas and Einaudi (1976), the possible wavelengths of the shear-induced gravity wave are 10.9 km (mode I), 20.0 km (mode II) and 29.6 km (mode III). These wavelengths are larger than the observed wavelength. However, if we assume that the wave developed above 2.8 km, as indicated in Fig. 7, the calculated wavelengths are 6.8 km (mode I), 12.6 km (mode II), 18.5 km (mode III). Since the sounding data at Lindenberg were not sufficiently reliable, especially in height resolution, mode I could account for the observed wavelength. In fact, Gultepe and Starr (1995) reported that gravity waves were more frequently found of scales between 2 and 9 km.

Figure 1b shows another small-scale structure, that is, a large increase of updraught velocity above 4.0 km and several maxima in the updraught region, indicating intermittent convection. In their numerical experiments, Starr and Cox (1985 b) also pointed out that the cells in the cirrus case appear more as rising bubbles or puffs than the more sustained thermals seen in the altostratus case. The intermittent updraught apparently did not originate in the convective echo region (above 4.6 km), but in the streak region (~4 km) and below the thermally-unstable layer.

A strong interaction between convection and formation of gravity waves in the stable layer below has been suggested by many researchers (Carbone and Bohne, 1975; Heymsfield, 1975 a; Testud et al., 1980; Wang et al., 1983; Starr and Cox, 1985 a; Auria and Campistron, 1987; Sassen et al., 1989; Heymsfield et al., 1990; Starr and Wyle, 1990; Quante, 1989; Gultepe et al., 1995; Gultepe and Starr, 1995; Kropfli and Kelly, 1996). However, our case exemplified this strong connection directly.

6.2 Microphysical structure of the ice cloud

The vertical profile of radar reflectivity is an indication of microphysical processes in a cloud. The time-averaged vertical distribution of radar reflectivity (10Log Z_e) in Fig. 8 shows that this value increased strongly with decreasing altitude from 5.2 to 4.9 km, and continued to increase from 4.9 to 4.6 km (in the convective echo region). From 4.6 to 3.4 km (in the streak region), 10Log Z_e increased only slightly. Therefore precipitation particles are inferred to have grown mainly in the convective echo region. Between 3.0 and 2.7 km altitude (a layer with low relative humidity), 10Log Z_e decreased with decreasing altitude, suggesting the evaporation of particles.

Also shown in Fig. 8 is the time-averaged vertical distribution of the vertical Doppler velocity (V_D). Here, the positive sign of V_D means that particles move downward. 10Log Z_e increased slightly in the lower stratiform echo region (between 2.7 and 2.1 km, in layer II), then strongly below 2.1 km. V_D also decreased largely below 1.8 km, indicating the evaporation of precipitation particles at least below this altitude. The values of V_D in the lower stratiform echo region (below 2.5 km) were higher than in the convective and streak echo regions. In contrast, the values of 10 Log Z_e were much smaller in the lower layer than in the upper layer. This fact suggests that the difference in Doppler velocity can be ascribed to a difference in the type of particles or a difference in the mean vertical air velocity, as discussed in section 4.

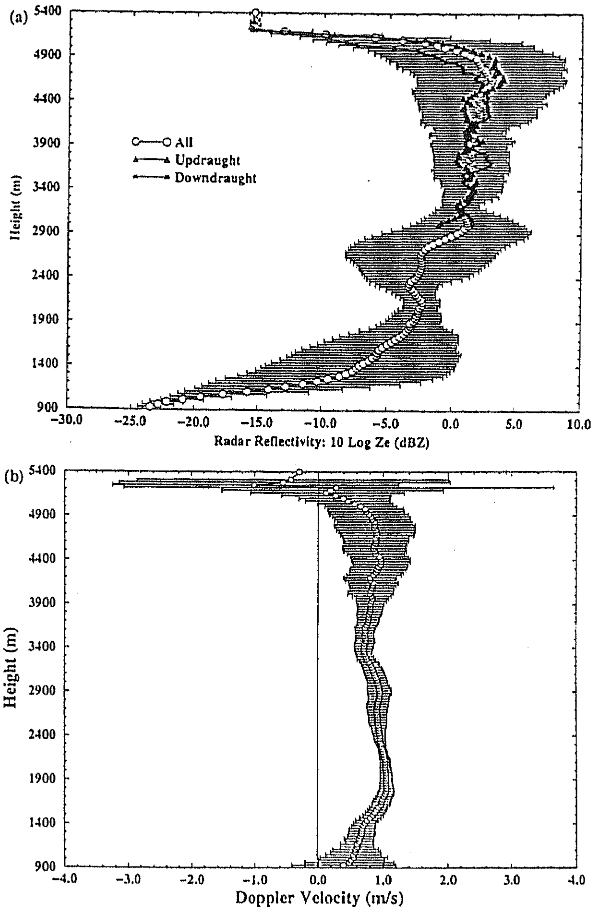

Figure 8: Vertical profiles of time-averaged radar reflectivity 10 Log Z_e (open circle; Fig. 8a) and vertical Doppler velocity (Fig. 8b). The horizon-tal bar shows the standard deviation. Vertical profiles of time-averaged radar reflec-tivities in updraught (black triangle) and downdraught (star) in the convective region are also shown in Fig. 8a. Positive sign of Doppler velocity in Figure 8b means downward motion of particles.

Convective-scale (1~0.5 km both in vertical and horizontal scales) up- and downdraughts were seen in the convective echo region in Figure 1b. The figure shows that the rising air parcels continued to exist near the cloud top even though downdraught was predominant below them. These air parcels would be able to survive until the air lost its buoyancy due to the entrainment of dry air caused by the small-scale and strong turbulence, and would be able to continue to produce precipitation particles.

Upward and downward Doppler velocities (Fig. 8b) and the values of PTKE (Fig. 5) increased drastically near the cloud top (above 5.1 km), similar to the observation of Gultepe et al. (1995). This result suggests that the forced convection near the cloud top amplified the vertical air motions, since the bulk Richardson number was ~1 above 5.0 km, due mainly to the strong wind shear. In addition to the convective-scale up- and downdraughts, small-scale ones (<100 m both in vertical and horizontal scales) were seen above 5.0 km, as shown in Figure 1b. This would correspond to the small-scale disturbance caused by strong wind shear (small-scale Kelvin-Helmholtz waves) as found by many researchers (e.g., Rayment and Readings, 1974; Heymsfield et al., 1990; Sassen et al., 1990).

As seen in Figure 1b, strong downdraughts existed between convective cells, that is, weak echo regions, and updraughts existed in convective cells. Thus, in general, there was a correlation between reflectivity and updraught as found by Carbone and Bohne (1975). From this result, they suggested that most of the particles are falling back through the updraught rather than diverging aloft into the downdraught. In our case, however, the organized downdraughts penetrated into the convective cells and below updraught regions. Further, strong reflectivities were also found in downdraught regions (as seen between altitudes of 4.0 and 4.5 km at the time mark of 90 seconds in Fig. 1). Therefore, particles grew both in updraught and downdraught regions.

The averaged vertical profiles of radar reflectivity in up- and downdraughts are also shown in Fig. 7a. Radar reflectivity in downdraughts was smaller than that in updraughts above 4.5 km on an average, which corresponds to the fact that the main downdraughts were formed in weak echo regions between generating cells. Radar reflectivity in updraughts increased rapidly with increasing altitude from 4.45 to 4.65 km. This fact indicates the existence of an accumulative layer of particles at the altitude of 4.65 km, as suggested by Sassen et al. (1989). Radar reflectivity decreased strongly above 4.9 km both in the updraughts and the downdraughts, indicating evaporation of ice particles due to entrainment of upper dry air in the cloud top area. Radar reflectivity in the downdraught increased more strongly with decreasing altitude than that in the updraught from 4.9 to 4.6 km in the convective echo region, indicating that particles in the downdraught grew faster than those in the updraught. In general, the amount of supercooled liquid water and the value of relative humidity are smaller in the downdraught than in the updraught. Therefore, the large increase in radar reflectivity with height in the downdraught suggests that precipitation particles increased their size during their fall by aggregation.

7 Summary and conclusion

This paper presents a case study of a deep stratiform ice cloud observed by the GKSS 95 GHz polarimetric Doppler radar. The altitudes of echo top and bottom were ~5.15 km (-30 ℃) and ~1 km (-7 ℃), respectively. Echo top level increased with increasing mean downdraught velocity. The cloud contained convective echoes above ~4.6 km, and typical streak echoes between 3 and 4.6 km. There was another thin stratiform radar echo below 2.5 km formed by weak ascending air motion.

The time-height cross section of the retrieved vertical air velocity indicates the occurrence of wave motion (wavelength ~3.6 km) of air in the streak region. The wave is suggested to be a gravity wave developed just above the lower stratiform echo. Just below the convective region, the general time-trend of vertical air velocity correlated well with the lower-level undulatory air motion. The intermittent updraught originated in the crest of the wave in the streak region (~4 km). The rising air parcels continued to survive and produce precipitation particles near the cloud top until the air loses its buoyancy. In addition to the convective-scale (0.5 ~ 1 km) up- and downdraughts, small-scale (<100m) ones existed near the cloud top, where the bulk Richardson number was ~1, due mainly to the strong wind shear. Their vertical air velocities did not correlate with the undulatory air motion below.

Radar reflectivity decreased strongly above 4.9 km both in the updraughts and the downdraughts, indicating evaporation of ice particles due to entrainment of upper dry air.

This study showed as an example the capabilities of a 95 GHz-radar to study the detailed dynamical and microphysical processes within ice clouds. However, further observations of various types of cloud systems by using the cloud radar and simultaneous *in situ* measurements are needed to confirm and evaluate the processes presented in this case study.

References

Atlas, D., S. Y. Matrosov, A. J. Heymsfield, M. D. Chou and D. B. Wolff, 1995: Radar and radiation properties of ice clouds. J. Appl. Meteor., 34, 2329-2345.

Auria, R. and B. Campistron, 1987: Origin of precipitation and dynamic organization in wavelike precipitation bands. J. Atmos. Sci., 22, 3329-3340.

Bluestein, H. B., A. L. Pazmany, J. C. Galloway, and R. E. McIntosh, 1995: Studies of the substructure of severe convective storms using a mobile 3-mm-wavelength Doppler radar. Bull. Amer. Meteor. Soc., 76, 2155 -2169.

Brown, P. R. A., A. J. Illingworth, A. J. Heymsfield, G. M. McFarquhar, K. A. Browning and M. Gosset, 1995: The role of spaceborne millimeter-wave radar in the global monitoring of ice cloud. J. Appl. Meteor., 34, 2346 -2366.

Carbone, R. E. and A. R. Bohne, 1975: Cellular snow generation - A Doppler radar study. J. Atmos. Sci., 32, 1384-1394.

Carbone, R. E. and R. C. Srivastava, 1975: Simultaneous aircraft and Doppler radar observations of a deep stratiform layer. Part II: Radar measurements and deduced air motions. Proc. 16th Radar Conf., Houston, 441-446.

Danne, O., G. G. Mace, E. E. Clothiaux, X. Dong, T. P. Ackerman and M. Quante,1996: Observing structures and vertical motions within stratiform clouds using a vertical pointing 94-GHz cloud radar. Beitr. Phys. Atmosph., 69, 229-237.

Gultepe, I., D. O'C. Starr, A. J. Heymsfield, T. Uttal, T. P. Ackerman, and D. L. Westphal, 1995: Dynamical characteristics of cirrus clouds from aircraft and radar observations in micro and meso-gamma scales. J. Atmos., Sci., 52, 4060-4078.

Gultepe, I. and D. O'C. Starr, 1995: Dynamical structure and turbulence in cirrus clouds: Aircraft observations during FIRE. J. Atmos. Sci., 52, 4159-4182.

Heymsfield, A., 1975a: Cirrus uncinus generating cells and the evolution of cirriform clouds. Part I: Aircraft observations of the growth of the ice phase. J.Atmos. Sci., 32, 799-808.

Heymsfield, A., 1975b: Cirrus uncinus generating cells and the evolution of cirriform clouds. Part II: The structure and circulations of the cirrus uncinus generating head. J. Atmos. Sci., 32, 809-819.

Heymsfield, A. J., K. M. Miller, and J. D. Spinhirne, 1990: The 27-28 October 1986 FIRE IFO cirrus case study: Cloud microstructure. Mon. Wea. Rev., 118, 2313 -2328.

Kropfli, R. A. and R. D. Kelly, 1996: Meteorological research applications of mm-wave radar. Meteorol. Atmos. Phys., 59, 105-121.

Lalas, D. P. and F. Einaudi, 1976: On the characteristics of gravity waves generated by atmospheric shear layers. J. Atmos. Sci., 33, 1248-1259.

Lhermitte, R., 1987: A 94-GHz Doppler radar for cloud observations. J. Atmos. Ocean. Tech., 4, 36-48.

Lhermitte, R. M., 1988: Cloud and precipitation remote sensing at 94 GHz. IEEE Trans. Geosci. Remote Sensing, 26, 207-216.

Matrosov, S. Y., T. Uttal, J. B. Snider and R. A. Kropfli, 1992: Estimation of ice cloud parameters from ground-based infrared radiometer and radar measurements. J.Geophys. Res., 97(D11), 11567-11574.

Matrosov, S. Y., B. W. Ott, R. A. Kropfli and J. B. Snider, 1994: Retrieval of vertical profiles of cirrus cloud microphysical parameters from Doppler radar and infrared radiometer measurements. J. Appl. Meteor., 33, 617-626.

Mead, J. B., A. L. Pazmany, S. M. Sekelsky and R. E. McIntosh, 1994: Millimeter-wave radars for remotely sensing clouds and precipitation. Proc. IEEE, 82, 1891-1905.

Pasqualucci, F., B. W. Bartram, R.A. Kropfli and W. R. Moninger, 1983: A millimeter-wavelength dual -polarization Doppler radar for cloud and precipitation studies. J. Clim. Appl. Meteor., 22, 758-765.

Pazmany, A. J., J. Mead, R. McIntosh, M. Hervig, R. Kelly, and G. Vali, 1994: 95-GHz polarimetric radar measurements of orographic cap clouds. J. Atmos. Oceanic Tech., 11, 140-153.

Quante, M. and P. R. A. Brown, 1992: Turbulence in different types of cirrus clouds. Proc. 11th International Conf. Clouds and Precipitation, Montreal, 17-22.

Quante, M., O. Danne, E. Raschke, I. Popstefanija and A. Pazmany, 1996: Observations of cloud structure with a 3.2 mm-wave radar. Proc. 12th International Conf. Clouds and Precipitation, Zurich, 424-427.

Sassen, K., 1987: Ice cloud content from radar reflectivity. J. Climate Appl. Meteor., 26, 1050-1053.

Sassen, K., D. O'C. Starr and T. Uttal, 1989: Mesoscale and microscale structure of cirrus clouds: Three case studies. J. Atmos. Sci., 46, 371-396.

Sassen. K., C. J. Grund, J. D. Spinhirne, M. M. Hardesty, and J. M. Alvarez, 1990: The 27-28 October 1986 FIRE IFO cirrus case study: A five lidar overview of cloud structure and evolution. Mon. Wea. Rev., 118, 2288-2311.

Sauvageot, H., 1992: Radar Meteorology. Atrech House, Inc., 366pp.

Sekelsky, S. M. and R. E. McIntosh, 1996: Cloud observations with a polarimetric 33 GHz and 95 GHz radar. Meteorol. Atmos. Phys., 59, 123-140.

Starr, D. O'C. and S. K. Cox, 1985a: Cirrus clouds. Part I: A cirrus cloud model. J. Atmos. Sci., 42, 2663-2681.

Starr, D. O'C. and S. K. Cox, 1985b: Cirrus clouds. Part II: Numerical experiments on the formation and maintenance of cirrus J. Atmos. Sci., 42, 2682-2694.

Starr D. O'C. and D. P. Wyle, 1990: The 27-28 October 1986 FIRE cirrus case study: Meteorology and clouds. Mon. Wea. Rev., 118, 2259-2287.

Stull, R. B., 1988: An Introduction to Boundary Layer Meteorology. Kluwer Academic Pub., 666pp.

Syrett, W. J., B. A. Albrecht, and E. E. Clothiaux, 1995: Vertical structure in a mid-latitude cyclone from a 94-GHz radar. Mon. Wea. Rev., 123, 3393-3407.

Testud, J., G. Breger, P. Amayenc, M. Chong, B. Nutten and Sauvageot, 1980: A Doppler radar observation of a cold front: three-dimensional air circulation, related precipitation system and associated wavelike motions. J. Atmos. Sci., 37, 78-98.

Uttal. T., E. E. Clothiaux, T. P. Ackerman, J. M. Intrieri, and W. L. Eberhard, 1995: Cloud boundary statistics during FIRE II. J. Atmos. Sci., 52, 4276-4284.